ISSN 1054-660X, Laser Physics, 2008, Vol. 18, No. 12, pp. 1435–1446.

Defect-Induced Instability of the Surface Layer Involving Static Coupled Lamb and Rayleigh Waves as a Universal Mechanism of the Formation of an Ensemble of Nanodot Nucleation Centers

V. I. Emel'yanov

Faculty of Physics, Moscow State University, Moscow, 119991 Russia

e-mail: emel@em.msk.ru

Received July 1, 2008

Abstract—It is demonstrated that a stressed flat surface nanolayer saturated with mobile point defects exhibits a threshold (with respect to the defect concentration or mechanical stress) transition to a periodic spatially bent state with a simultaneous formation of the spatially periodic defect pile-ups at the extrema of the spontaneously emerging surface relief. In this case, the layer deformation corresponds to the displacements in a static bending Lamb wave and the deformation of the underlying elastic continuum corresponds to the displacements in the static Rayleigh wave. For the first time, we demonstrate that the analysis simultaneously involving the nonlocal character of the defect interaction with the lattice atoms and both (normal and lateral) defect-induced forces that cause the bending of the surface layer yields two maxima on the curve of the instability growth rate versus the period of the generated relief. This corresponds to the experimentally observed two scales of the surface relief modulation upon the laser and ion irradiation of semiconductors. Based on the results obtained, we propose a cooperative defect–deformational (DD) mechanism for the formation of an ensemble of the nanoparticle nucleation centers above the critical levels of the stress or the defect concentration. An approach to the calculation of a bimodal distribution function of the nanoparticle nucleation centers with respect to their size is adequately developed to the DD mechanism of nucleation which represents the distribution function in terms of the growth rate. The calculated results are compared with the experimental data for the molecular beam epitaxy of the nanodot ensemble and the pulsed laser nanostructuring of a solid surface.

PACS numbers: 43.25.Rq, 66.30.Lw, 61.72.Yx, 68.55.Ln, 81.40.Lm, 61.80.Ba, 81.16.-c

DOI: 10.1134/S1054660X08120104

1. INTRODUCTION

Several processes of the nanostructure self-organization on solid surfaces are initiated from the generation of a surface nanolayer with mobile point defects (interstitials, vacancies, and doped atoms). For example, this scenario corresponds to the formation of a nanodot ensemble upon the laser and ion-beam irradiation of semiconductors and metals [1]. The radiation-induced surface layer that is saturated with defects has the lattice constant that differs from the lattice constant of the underlying crystal layer (substrate). This leads to a mechanical stress in the surface layer. We also consider the molecular-beam epitaxy (MBE) [2, 3] although the character of the defect-enriched layer and the defect type in this case need to be separately discussed (Section 5).

In this work, we analyze a flat tensile stressed surface layer saturated with mobile point defects and demonstrate that the flat state becomes unstable above certain critical levels of the stress or the defect concentration and the layer exhibits a transition to a periodically bent state with the simultaneous accumulation of defects at the relief extrema. The material displacements inside the layer and the substrate are determined as in the bending Lamb wave and the Rayleigh wave, respectively. The resulting coupled static Lamb–Rayleigh deformations in the layer and the substrate are maintained due to the self-consistent distribution of the point defects that deform the elastic continuum. Such a deformed state of the layer and the substrate represents a static analog of a dynamic Lamb–Rayleigh wave that propagates in a thin surface layer whose density is higher than the substrate density [4].

The generation of a periodic surface relief is accompanied by the defect pile-ups at the relief extrema. Note that interstitials and vacancies accumulate at the hills and wells of the relief, respectively. Such a periodic modulation of the surface relief and the coupled grating of the defect pile-ups constitute the surface defect–deformational (DD) grating with wave vector $\mathbf{q}$. When the DD instability is developed, the DD-grating amplitudes increase with time as $\exp(\lambda_\mathbf{q} t)$, where $\lambda_\mathbf{q}$ is the growth rate. The value $q = q_\mathrm{m}$ corresponding to the maximum growth rate determines the period of dominant gratings $\Lambda_\mathrm{m} = 2\pi/q_\mathrm{m}$ which are selected in the Fourier spectrum of the surface relief.

A superposition of the surface DD gratings with different $\mathbf{q}$ yields a cellular seed DD structure on the sur-

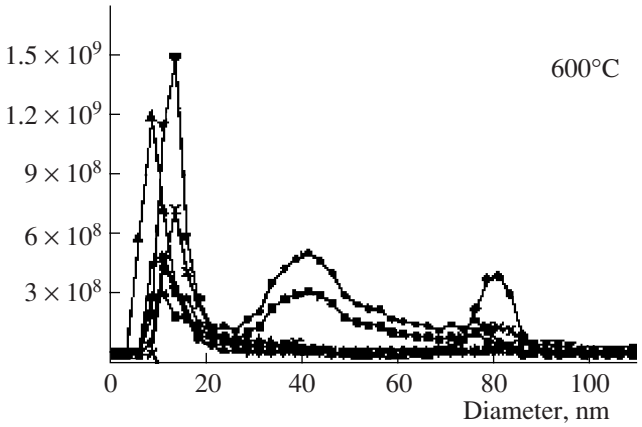

Fig. 1. Ge/Si (100) island size distribution for several Ge coverages [5]: (circles) 5.0, (squares) 6.5, (triangles) 8.0, (crosses) 9.5, (inverted triangles) 11.0, and (diamonds) 12.5 ML.

face [1]. The characteristic scale of heterogeneities therein is determined by Λ_m and the symmetry depends on the selection of the **q** vector directions. At a relatively high intensity of the laser or ion irradiation, this seed structure is etched, so that the regions of the defect accumulation are etched at a rate that differs from the etching rates in other regions. The etching leads to the visualization of the seed DD structure, which imposes its periodicity and symmetry on the resulting structure of the surface relief [1].

In this work, we demonstrate for the first time that the analysis simultaneously involving the nonlocal character of the defect interaction with the crystal-lattice atoms up to the fourth-order term in the expansion of the kernel of the interaction operator and both (normal and lateral) defect-induced forces that cause the layer bending yields two maxima on the curve of the instability growth rate versus relief period Λ sufficiently far above the instability threshold (far above the critical defect concentration or the critical stress). In contrast, the growth rate only exhibits a single maximum not far above the threshold. When the periodic surface relief is induced by energy beams, two maxima of the growth rate must give rise to two scales of the relief modulation with the large(micron)-scale modulation supplementing the small(nano)-scale modulation. These two scales of the surface relief modulation are characteristic of the nanorelief self-organization upon both laser and ion-beam irradiation of semiconductors [1].

In the case of the MBE, the strain extrema in the seed superpositional DD structure with different periods Λ serve as the nanodot nucleation centers. The growth of nucleuses in these centers results in the formation of a nanodot ensemble. In this case, the seed DD relief is visualized owing to the nucleation and the nanoparticle growth.

In this work, we develop a new approach to the calculation of the size distribution function of the nucle-

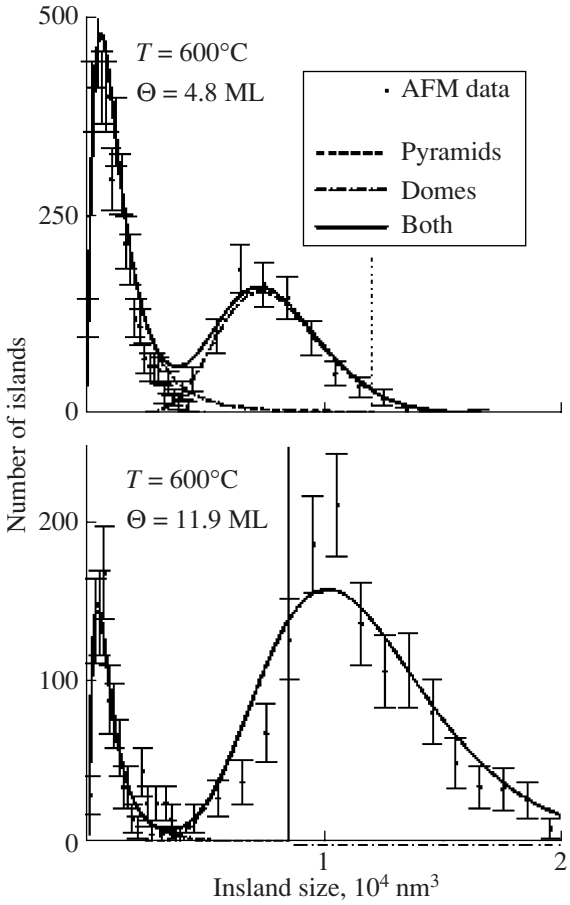

Fig. 2. Size distribution of the Ge islands for two Ge coverages resulting from the AFM data [3].

ation centers. This approach is adequate for the cooperative DD character of the formation of the nucleation center ensemble and makes it possible to represent the distribution function in terms of the DD instability growth rate $\lambda(\Lambda)$. Function $\lambda(\Lambda)$ exhibits one or two maxima depending on the growth conditions. Therefore, the calculated function $n_{dot}(\Lambda)$ also exhibits one or two maxima. It is known that, in the case of the MBE, the size distribution function of nanodots is transformed from the unimodal to bimodal representation [3, 5]. In the last case, the distribution function has a specific shape with a relatively broad quasi-symmetric maximum in the region of relatively large nanoparticle sizes and a narrower asymmetric intense maximum in the region of small sizes of nanoparticles (Figs. 1 and 2). The shape of the bimodal distribution function $n_{dot}(\Lambda)$ obtained in this work and the predicted positions of the maxima correspond to the experimental distribution function. Note that, under certain regimes of the pulsed laser nanostructuring of solid surfaces, the size distribution function of nanohills also exhibits a transition from the unimodal to bimodal shape upon a variation in the irradiation regime [6] (Fig. 3). In this work, this effect is interpreted in the framework of a universal

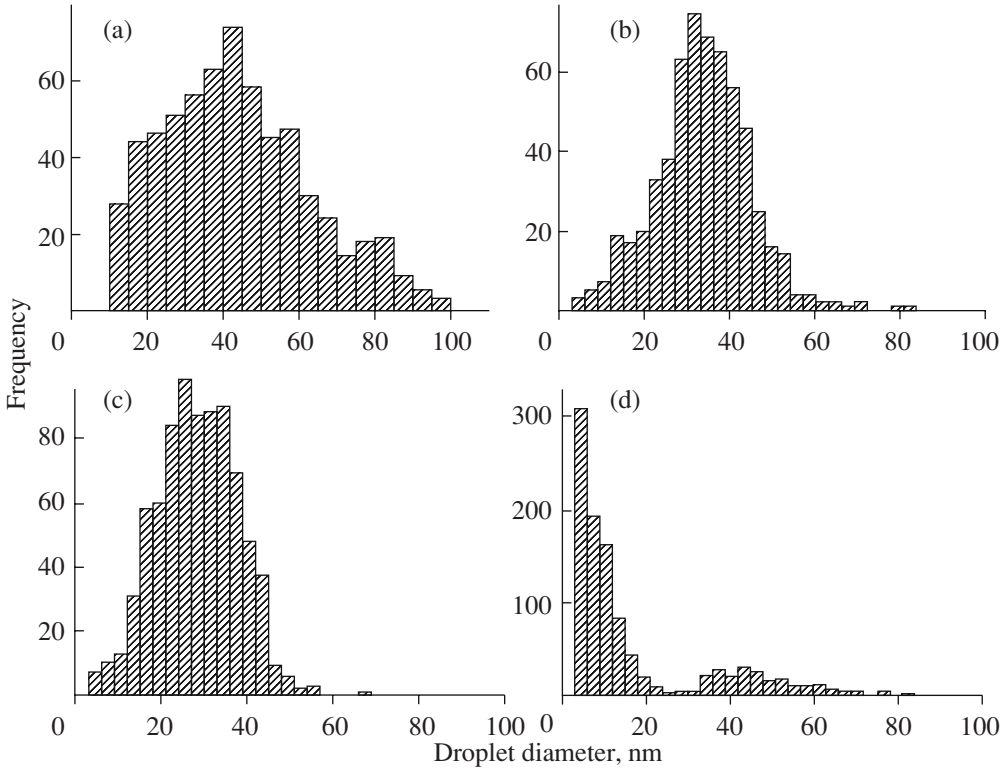

Fig. 3. Diameter distribution of the Ag nanoparticles created by the multipulse excimer laser microstructuring of a thin (5-nm-thick) Ag-on-oxide film at fluences of (a) 175, (b) 250, (c) 400, and (d) 600 mJ cm^{-2} [6].

DD mechanism for the self-organization of the nucleation-center ensemble upon the laser action (etching) and MBE.

2. EQUATIONS OF THE DD INSTABILITY OF THE STRESSED LAYER WITH MOBILE DEFECTS ON THE SUBSTRATE

We assume that the laser irradiation of a crystal or the deposition of a layer on the substrate using the MBE leads to the generation of point defects with concentration n_d (d = v and i for vacancies and interstitials, respectively) in the surface layer with thickness h. The plane $z = 0$ coincides with the free surface of the sample and the z axis is directed from the surface to the bulk.

The spatial distribution of the defect concentration is written as

$$n_\mathrm{d}(x, y, z, t) \equiv N_\mathrm{d}(x, y, t) f(z), \tag{1}$$

where $N_\mathrm{d}(x, y, t)$ is the surface concentration of the defects and function $f(z)$ that determines the defect distribution along the normal to the layer will be defined below (see expression (15)).

The equations of the model are written on the assumption of the isotropic surface diffusion and drift. The surface flux of defects $\mathbf{j}_\mathrm{d}$ consists of the diffusion- and deformation-induced components:

$$\mathbf{j}_\mathrm{d} = -D_\mathrm{d}\nabla N_\mathrm{d} + N_\mathrm{d}\frac{D_\mathrm{d}}{k_\mathrm{B}T}\mathbf{F}(\mathbf{r}). \tag{2}$$

Here, the lateral nonlocal force that is exerted on the defect by the deformed elastic continuum is given by

$$\mathbf{F}(\mathbf{r}) = \theta_\mathrm{d}\nabla_\parallel(\xi_\mathrm{f} + l_\mathrm{d}^2\Delta_\parallel\xi_\mathrm{f} + L_\mathrm{d}^4\Delta_\parallel^2\xi_\mathrm{f})_{z=0}, \tag{3}$$

where $\mathbf{r} = (x, y)$, $\nabla_\parallel \equiv \mathrm{grad}_\parallel = \hat{e}_x\frac{\partial}{\partial x} + \hat{e}_y\frac{\partial}{\partial y}$ ($\hat{e}_x$ and $\hat{e}_y$ are unit vectors along the x and y axes), $\theta_\mathrm{d} = \Omega_\mathrm{d}K$ is the deformation potential of the defect, Ω_d is a variation in the volume of the medium due to the formation of one defect, K is the elasticity modulus, $\xi_\mathrm{f} = \xi_\mathrm{f}(x, y, z) = (\mathrm{div}\,\mathbf{u}_\mathrm{f})$ is the strain in the layer, and $\mathbf{u}_\mathrm{f} = \mathbf{u}_\mathrm{f}(x, y, z, t)$ is the material displacement vector in the layer. In formula (3), we introduce two new parameters that were previously missing in the DD theory [1]: parameters l_d^2 and L_d^4 describe the nonlocal defect interaction with the lattice atoms. The nonlocality parameters l_d and L_d are assumed to be given parameters. In the microscopic approach, they result from the expansion of the nonlocal deformation that enters the integrand along with the interaction kernel that decays at the characteristics lengths of the

defect–atom interaction (~l_d and L_d). The typical values are several nanometers (see, for example, [7]).

Using expression (3) in the continuity equation for N_d, we obtain the surface-diffusion equation allowing for the strain-induced drift of the defects:

$$\frac{\partial N_d}{\partial t} = D_d\Delta_\parallel N_d - \frac{N_d}{\tau_d} - \frac{D_d\theta_d}{kT_B}\mathrm{div}[N_d\nabla_\parallel(\xi_f + l_d^2\Delta_\parallel\xi_f + L_d^4\Delta_\parallel^2\xi_f)]_{z=0}, \quad (4)$$

where $\Delta_\parallel = \frac{\partial^2}{\partial x^2} + \frac{\partial^2}{\partial y^2}$, D_d is the surface diffusion coefficient, and τ_d is the defect lifetime. We neglect the renormalization of the diffusion coefficient due to the deformation.

To find $\xi_f = \mathrm{div}\,\mathbf{u}_f$, we will consider the defect-enriched layer with thickness h as a film with density ρ and Young modulus E. The film is connected to the substrate (the remaining part of the crystal) with elastic parameters ρ_s and E_s. The free surface of the film is $z = 0$, and the deformation in the substrate is described using the material displacement vector $\mathbf{u}(x, y, z, t)$. We assume that the film exhibits the bending deformation and that the z component of the film displacement vector is $u_{f_z} = \zeta(x, y)$, where ζ is the bending coordinate of the film (the z displacement of the points on the median plane of the film from the equilibrium position).

The shear stresses in the film and in the substrate are equal to each other at $z = h$:

$$\mu_f(z=h)\left(\frac{\partial u_{fx_\alpha}}{\partial z} + \frac{\partial u_{fz}}{\partial x_\alpha}\right)_{z=h} = \mu_s(z=h)\left(\frac{\partial u_{x_\alpha}}{\partial z} + \frac{\partial u_z}{\partial x_\alpha}\right)_{z=h}, \quad (5)$$

where $x_\alpha = \{x, y\}$, $\mu_f(z = h)$, and $\mu_s(z = h)$ are shear moduli in the film and substrate, respectively, at $z = h$.

We assume that $\mu_s(z = h) \longrightarrow 0$ due to the generation of dislocations (e.g., misfit dislocations) at the film–substrate interface. Then, expression (5) yields $\mu_f(z = h)(\partial u_{fx_\alpha}/\partial z + \partial u_{fz}/\partial x_\alpha)_{z=h} = 0$. The same zero boundary condition for the shear component of the stress tensor is satisfied at the free film surface $z = 0$. In addition, to determine the film deformation in the zero approximation with respect to the substrate reaction along the normal, we assume that the normal component of the stress tensor in the film is zero at the interface:

$$\sigma_{fzz}(x, y, z = h) \equiv (\sigma_f)_\perp = 0. \quad (6)$$

At the free surface, we also have $\sigma_{fzz}(x, y, z = 0) = 0$. Note that a conventional approximation in the theory of thin-film bending [8] implies that the external force exerted along the normal to the film is neglected in the boundary condition upon the derivation of the thin-film deformation under the action of this force. Thus, in the above approximation, the free-film condition $\sigma_{fxz} = \sigma_{fyz} = \sigma_{fzz} = 0$ is satisfied on both film interfaces. Then, the film strain $\xi_f = \mathrm{div}\,\mathbf{u}_f$ is represented as [8]

$$\xi_f = -\nu\left(z - \frac{h}{2}\right)\Delta_\parallel\zeta, \quad (7)$$

where $\nu = (1 - 2\sigma_P)/(1 - \sigma_P)$, σ_P is the Poisson coefficient of the film, and $\Delta_\parallel = \frac{\partial^2}{\partial x^2} + \frac{\partial^2}{\partial y^2}$. The linear sign-alternating deformation in the layer as a function of z (expression (7)) is characteristic of the Lamb wave in plates [4].

Substituting expression (7) in formula (4), we derive the equation

$$\frac{\partial N_d}{\partial t} = D_d\Delta_\parallel N_d - \frac{N_d}{\tau_d} - \frac{\nu h D_d\theta_d}{2kT_B}\mathrm{div}[N_d\nabla_\parallel(\Delta_\parallel\zeta + l_d^2\Delta_\parallel^2\zeta + L_d^4\Delta_\parallel^3\zeta)]. \quad (8)$$

Aiming to find the growth rate of the DD structure, we restrict consideration to the initial (linear) regime of the DD instability. The following linear equation for the ζ coordinate follows from the generalization of the conventional equation for the bending of a free film [8]:

$$\frac{\partial^2\zeta}{\partial t^2} + l_0^2c^2\Delta_\parallel^2\zeta - \frac{\sigma_\parallel}{\rho_f}\Delta_\parallel\zeta = \frac{\sigma_\perp}{\rho_f h} - \sum_d\left\{-\frac{\theta_d}{\rho_f h}\int_0^h\frac{\partial n_d}{\partial z}dz + \frac{\nu\theta_d}{\rho_f h}\int_0^h\left(z - \frac{h}{2}\right)\Delta_\parallel n_d dz\right\}, \quad (9)$$

where $c^2 = E_f/\rho_f(1 - \sigma_f^2)$ is the film rigidity, E_f is the Young modulus, and $l_0^2 = h^2/12$. The summation on the right-hand side involves vacancies (d = v) and interstitials (d = i). Note that the film bending rigidity (the coefficient of $\Delta_\parallel^2\zeta$) depends on film thickness h that serves as a scale parameter specific of the DD instability.

The generalization of the conventional bending equation is as follows. On the left-hand side of expression (9), the term proportional to ~$\sigma_\parallel$ takes into account the effect of the isotropic lateral stress in the film resulting from the misfit of the lattice parameters of the film and the substrate and/or the defect generation in the surface layer. We assume that $\sigma_\parallel > 0$, so that the film is under tensile stress which is assumed to be known. In the first term on the right-hand side of expression (9), $\sigma_\perp$ is the stress that is normal to the film surface and that arises due to the substrate action on the film (substrate

reaction). Note that in the analysis of the film bending, expression (9) takes into account the substrate reaction, which has previously been neglected in the analysis of the internal deformations in the film. Such an approach is not controversial and can be substantiated. The second term on the right-hand side of formula (9) takes into account the defect-induced bending force that acts along the normal to the film surface due to the nonuniform distribution of the defects along the z axis. The third term on the right-hand side takes into account the defect-induced bending lateral force resulting from the nonuniform distribution of the defects along the film. Thus, Eq. (9) takes into account both forces (normal and tangential) exerted on the film by the defect subsystem.

The film bending gives rise to displacement vector $\mathbf{u}$ in the substrate, which is given by

$$\frac{\partial^2 \mathbf{u}}{\partial t^2} = c_t^2 \Delta \mathbf{u} + (c_l^2 - c_t^2)\mathrm{grad}\,\mathrm{div}\,\mathbf{u}, \quad (10)$$

where c_l and c_t are longitudinal and transverse velocities of sound in the substrate, respectively.

We have three boundary conditions at the film–substrate interface. The z displacement is continuous, so that

$$u_z(z = h) = \zeta. \quad (11)$$

The normal stress in the substrate determines the force exerted on the film along the z axis:

$$\left[\frac{\partial u_z}{\partial z} + (1 - 2\beta_s)\left(\frac{\partial u_x}{\partial x} + \frac{\partial u_y}{\partial y}\right)\right]_{z = h} = \frac{\sigma_\perp(x, y)}{\rho_s c_l^2}, \quad (12)$$

where $\beta_s = c_t^2/c_l^2$.

The tangential stress at the interface is zero:

$$\left(\frac{\partial u_{x_\alpha}}{\partial z} + \frac{\partial u_z}{\partial x_\alpha}\right)_{z = h} = 0, \quad (13)$$

where $x_\alpha = \{x, y\}$.

We do not impose limitations on the tangential components of the displacement vector in the substrate at the interface $u_{x_\alpha}(z = h)$. This assumption and condition (13) follow from the assumption on the generation of the misfit dislocations at the interface.

System of equations (8)–(13) represents a closed system of equations that describes the DD instability of a stressed flat thin surface layer with mobile defects. We demonstrate below that such an instability is related to the defect-induced instability of the static Lamb waves in the layer coupled with the static Rayleigh waves in the underlying elastic continuum.

3. TWO MAXIMA OF THE GROWTH RATE OF THE SURFACE DD GRATINGS AS FUNCTIONS OF THE WAVE NUMBER

The defect concentration at the surface is represented as

$$N_d(x, y, t) = N_{d0} + N_{d1}(x, y, t),$$

where N_{d0} and $N_{d1}(x, y, t)$ are the spatially uniform and nonuniform components, respectively, of the defect concentration ($N_{d1}(x, y, t) \ll N_{d0}$). Linearizing expression (6) and using formula (7), we derive an equation for $N_{d1}(x, y, t)$ neglecting (for simplicity) the defect recombination:

$$\frac{\partial N_{d1}}{\partial t} = D_d \Delta_\parallel N_{d1} - D_d B N_{d0} \Delta_\parallel^2 [\zeta + l_d^2 \Delta_\parallel \zeta + L_d^4 \Delta_\parallel^2 \zeta], \quad (14)$$

where $B = \dfrac{\nu \theta_d h}{2kT_B}$.

We also employ $n = n_{d0} + n_{d1}$, where n_{d0} and n_{d1} are spatially uniform and nonuniform components of the defect concentration, respectively. Since $h \ll \Lambda$, n_{d1} is rapidly adjusted to the z distribution of the bending deformation and is given by the antisymmetric function in terms of z:

$$n_{d1}(x, y, z, t) = \frac{2}{h}\left(\frac{h}{2} - z\right)N_{d1}(x, y, t). \quad (15)$$

Thus, we obtain

$$n_{d1}(z = 0) = -n_{d1}(z = h) = N_{d1}. \quad (16)$$

Substituting expression (15) to the right-hand side of relationship (9) and calculating the integrals with regard to expression (16), we obtain the following equation assuming that the deformation is instantaneously adjusted to the defect subsystem $\left(\dfrac{\partial^2 \zeta}{\partial t^2} = 0\right)$:

$$\Delta_\parallel^2 \zeta - \frac{1}{l_\parallel^2}\Delta_\parallel \zeta = \frac{\sigma_\perp}{\rho_f c^2 h l_0^2} - \sum_d \left(A_d - \frac{\nu \theta_d}{\rho_f c^2 h}\Delta_\parallel\right)N_{d1}, \quad (17)$$

where $A_d = \dfrac{2\theta_d}{h l_0^2 \rho_f c^2}$ and the characteristic scale parameter is given by

$$l_\parallel = h\left(\frac{\rho_f c^2}{12\sigma_\parallel}\right)^{1/2}.$$

To eliminate substrate reaction $\sigma_\perp$ in the system of equations (14) and (17), we search for a solution to

boundary problem (10)–(13). In expression (12), we employ the Fourier-series expansion:

$$\sigma_\perp = \sigma_\perp(\mathbf{r}, t) = \sum_{\mathbf{q}} \sigma_\perp(q)\exp(i\mathbf{qr} + \lambda_q t).$$

We search for the displacement vector in the substrate that satisfies Eq. (10) as a superposition of quasi-Rayleigh (static) waves that represent modifications of the surface acoustic Rayleigh waves [8]. Each displacement vector in this superposition is represented as a sum of the longitudinal and transverse components ($\mathbf{u} = \mathbf{u}_\mathrm{l} + \mathbf{u}_\mathrm{t}$), which satisfy the conditions $\mathrm{curl}(\mathbf{u}_\mathrm{l}) = 0$ and $\mathrm{div}(\mathbf{u}_\mathrm{t}) = 0$. For the longitudinal component, we have

$$\begin{aligned} u_{\mathrm{l}x_\alpha} &= -i\sum_{\mathbf{q}} q_{x_\alpha} R(q)\exp(i\mathbf{qr} - k_\mathrm{l} z + \lambda_q t), \\ u_{\mathrm{l}z} &= \sum_{\mathbf{q}} k_\mathrm{l} R(q)\exp(i\mathbf{qr} - k_\mathrm{l} z + \lambda_q t). \end{aligned} \tag{18}$$

For the transverse component, we obtain

$$\begin{aligned} u_{\mathrm{t}z\alpha} &= -i\sum_{\mathbf{q}} \frac{q_{x_\alpha}}{q} k_\mathrm{t} Q(t)\exp(i\mathbf{qr} - k_\mathrm{t} z + \lambda_q t), \\ u_{\mathrm{t}z} &= \sum_{\mathbf{q}} q Q(t)\exp(i\mathbf{qr} - k_\mathrm{t} z + \lambda_q t), \end{aligned} \tag{19}$$

where $k^2_{\mathrm{l,t}} = q^2 + \lambda_q^2/c^2_{\mathrm{l,t}}$ and $R(q)$ and $Q(q)$ are the fluctuation amplitudes. It follows from expressions (18) and (19) that the frequency is $\omega_q = 0$ in the static quasi-Rayleigh wave.

The solution of system of equations (10)–(13) in the Fourier representation yields the relationship

$$\zeta_q\left\{\frac{2k_\mathrm{l}k_\mathrm{t} - k_\mathrm{t}^2 - q^2}{(k_\mathrm{t}^2 - q^2)k_\mathrm{l}}(q^2 + k_\mathrm{t}^2) - 2k_\mathrm{t}\right\} = \frac{\sigma_\perp(q)}{\rho_\mathrm{s} c_\mathrm{t}^2}.$$

Using the expansion of the expression in braces in terms of the small parameter $\lambda_q^2/c^2_{\mathrm{l,t}}q^2 \ll 1$, we find the reaction stress of the substrate caused by the film bending:

$$\sigma_\perp(q) = \zeta_q 2q(\beta_\mathrm{s} - 1)\rho_\mathrm{s} c_\mathrm{t}^2. \tag{20}$$

Below, we employ the Fourier-series expansions

$$\zeta(\mathbf{r}, t) = \sum_{\mathbf{q}} \zeta_\mathbf{q}\exp(i\mathbf{qr} + \lambda_q t), \tag{21}$$

$$N_{\mathrm{d}1}(\mathbf{r}, t) = \sum_{\mathbf{q}} N_\mathrm{d}(\mathbf{q})\exp(i\mathbf{qr} + \lambda_\mathrm{q} t). \tag{22}$$

Formulas (21) and (22) determine the superpositional DD structure consisting of the coupled 2D (cellular) DD gratings of the surface relief and defect concentration, respectively. Each DD grating with wave vector $\mathbf{q}$ can be interpreted as the bending static Lamb wave with the wavelength $\Lambda = 2\pi/q$ that is maintained by the self-consistent distribution of the defects. Each Lamb wave (21) is related to the static Rayleigh wave with the same wave vector $\mathbf{q}$ from superposition (18) and (19). The Fourier amplitudes of each DD grating with wave vector $\mathbf{q}$ and the coupled Rayleigh wave increase in time with growth rate λ_q. The summations in superpositions (21) and (22) as well as in superpositions (18) and (19) involve both directions and magnitudes of vectors $\mathbf{q}$. Note that the summation with respect to the magnitude $|\mathbf{q}| = q$ is performed in the limits $q_1 \le q \le q_\mathrm{c}$, where $q_1 = \pi/L$ is the wave number of the first bending mode (L is the lateral size of the region with mobile defects) and $q_\mathrm{c} = \pi/h$ is the wave number of the limiting bending mode. In the last case, the periodically bent film represents an accordion-type structure with the period $\Lambda_\mathrm{c} = 2h$ of the corresponding modulation of the surface relief.

Using expressions (15)–(17), we find the linear dependence of $\zeta_\mathbf{q}$ on $N_\mathrm{d}(\mathbf{q})$ for the DD grating with wave vector $\mathbf{q}$:

$$\zeta_\mathbf{q} = \sum_\mathrm{d} \eta_\mathrm{d}(\mathbf{q}) N_\mathrm{d}(\mathbf{q}), \tag{23}$$

where the coefficient of the DD coupling in the linear approximation is given by

$$\begin{aligned} \eta_\mathrm{d}(\mathbf{q}) &= -\frac{2\theta_\mathrm{d}}{\rho_\mathrm{f} c^2 h l_0^2}(1 + \nu l_0^2 q^2) \\ &\times \left[q^4 + l_\parallel^{-2} q^2 + \frac{2(1 - \beta_\mathrm{s})\mu_\mathrm{s}}{h l_0^2 \rho_\mathrm{f} c^2} q\right]^{-1}. \end{aligned} \tag{24}$$

To derive this formula, we employ the relationship $\mu_\mathrm{s} = \rho_\mathrm{s} c_\mathrm{t}^2$.

The term in parentheses in expression (24) takes into account the bending effect of two defect-induced forces (compare with expression (9)). In the denominator in expression (24), the first two terms take into account the effective bending rigidity of the film allowing for the lateral stress in the film (the term proportional to $\sim l_\parallel^{-2}$). The last term in the denominator, which is proportional to $\sim\mu_\mathrm{s}$, takes into account the reaction of the elastic substrate to the film bending. Neglecting this effect, we arrive at a simplified DD model (the model of a free film with mobile defects), in which the coefficient of the DD coupling is represented as

$$\eta_\mathrm{d}(\mathbf{q}) = -\frac{2\theta_\mathrm{d}}{\rho_\mathrm{f} c^2 h l_0^2}(1 + \nu l_0^2 q^2)[q^4 + l_\parallel^{-2} q^2]^{-1}. \tag{25}$$

The comparison of expressions (24) and (25) yields the condition under which the substrate reaction can be neglected: $\sigma_\parallel > 2(1 - \beta_s)\mu_s/qh$. In accordance with the assumption for the case under study, the shear modulus decreases due to the generation of the misfit dislocations. Thus, the substrate reaction can be neglected at a relatively large stress $\sigma_\parallel$.

For simplicity, we only consider the contribution of the defects of one type in formula (23). Substituting expressions (23) and (25) in the Fourier transform of expression (14), we find the growth rate of the DD grating:

$$\lambda_{\mathbf{q}} = -D_d q^2 + D_d q^2 \frac{N_{d0}}{N_c} \frac{(1 + \nu l_0^2 q^2)[1 - l_d^2 q^2 + L_d^4 q^4]}{1 + l_\parallel^2 q^2}, \quad (26)$$

where we introduce the critical concentration of the defects

$$N_c = \sigma_\parallel \frac{k_B T}{\nu \theta_d^2}. \quad (27)$$

The first and second terms in the parentheses in the numerator of expression (26) correspond to the normal and tangential defect-induced bending forces, respectively, exerted on the film. The first term in the brackets in the numerator of expression (26) takes into account the local force exerted by the deformation of the elastic continuum on the defect, and the remaining terms proportional to $\sim l_d^2$ and L_d^4 take into account the nonlocal character of this force. Figures 4a and 4b demonstrate the plots of the growth rate $\lambda_{\mathbf{q}} \equiv \lambda(\Lambda)$ calculated using expression (26) at two values of the control parameter $N_{d0}/N_c = 50$ and 100, respectively. The following parameters were used in the calculations: $h = 10^{-6}$ cm, $\rho_f c^2 = 7 \times 10^{11}$ erg cm^{-3}, $\sigma_\parallel = 10^{10}$ erg cm^{-3}, $\nu = 1$, $l_d = L_d = 3 \times 10^{-7}$ cm, and $D_d = 10^{-14}$ cm^2 s^{-1}.

It follows from Fig. 4 that the growth rate exhibits a single maximum at $\Lambda = \Lambda_m$ at sufficiently high concentrations of the defects exceeding the threshold value and that an additional maximum emerges in the short-wavelength range at $\Lambda < \Lambda_c = 2h = 2 \times 10^{-6}$ cm when the concentration is further increased. Therefore, two DD gratings with $\Lambda = \Lambda_m$ and $\Lambda = \Lambda_c$ have the maximum growth rates.

The long-wavelength maximum of the growth rate with $\Lambda = \Lambda_m$ (at $q = q_m$) can be analytically described provided that the nonlocal character of the DD interaction is neglected in expression (26) (i.e., $l_d = L_d = 0$) and the lateral bending force is also neglected ($\nu l_0^2 q^2 < 1$). Then, using expression (26), we have

$$\lambda_{\mathbf{q}} = -D_d q^2 + D_d q^2 \frac{N_{d0}}{N_c} \frac{1}{1 + l_\parallel^2 q^2}. \quad (28)$$

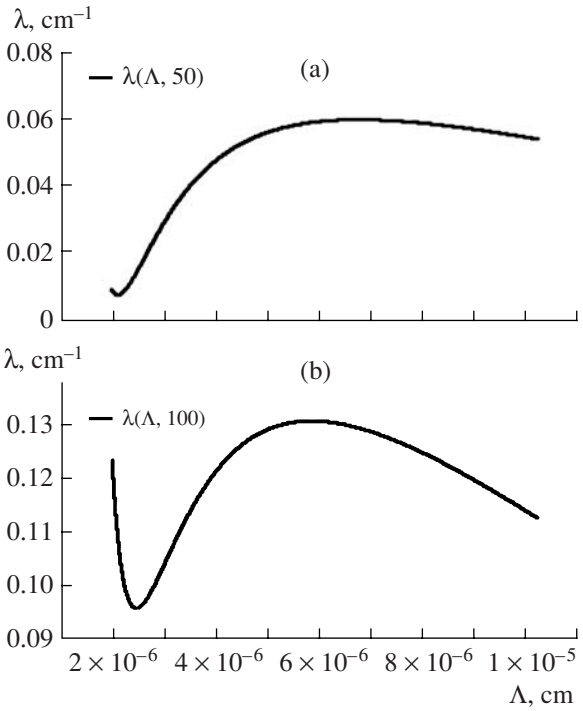

Fig. 4. Plots of the growth rate λ for the Fourier amplitude of the DD grating vs. grating period Λ calculated using formula (26) for the values of control parameter $\frac{N_{d0}}{N_c}$ = (a) 50 and (b) 100.

The maximum on the curve λ_q is reached at $q = q_m$ and

$$q_m = \frac{1}{l_\parallel}\left(\left(\frac{N_{d0}}{N_c}\right)^{1/2} - 1\right)^{*\dagger\ddagger}. \quad (29)$$

The corresponding period of the dominant DD grating with wave vector q_m is given by

$$\Lambda_m = 2\pi/q_m = 2\pi h\left(\frac{\rho_f c^2}{12\sigma_\parallel}\right)^{1/2} \frac{1}{((N_{d0}/N_c)^{1/2} - 1)^{1/2}} \quad (29a)$$

and is proportional to layer thickness h.

The maximum growth rate for the grating with $q = q_m$ is

$$\lambda_m = D_d q_m^2 (\sqrt{N_{d0}/N_c} - 1) = \frac{D_d (\sqrt{N_{d0}/N_c} - 1)^2}{l_\parallel^2} \operatorname{sgn}(\sqrt{N_{d0}/N_c} - 1). \quad (30)$$

It follows from expressions (23) and (24) that a real value of q_m emerges and growth rate λ_m becomes positive when the critical concentration of the defects is exceeded ($N_{d0}/N_c > 1$). For $T = 600$ K, $\theta_d = 10^2$ eV, $\sigma_\parallel = 10^{10}$ erg cm^{-3}, and $\nu = 1$, expression (27) yields the critical concentration $N_c = 2 \times 10^{16}$ cm^{-3}.

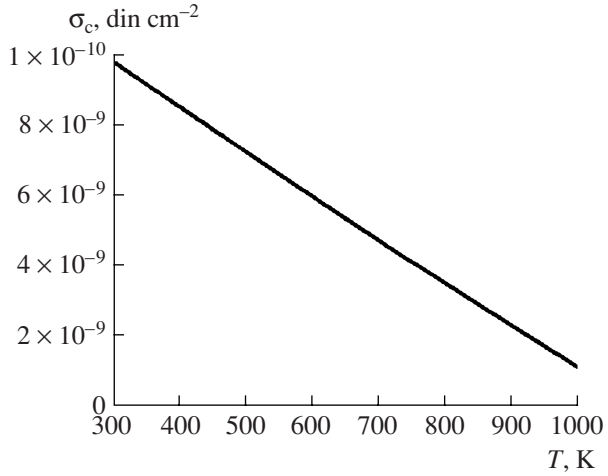

Fig. 5. Plot of critical stress σ_c in the surface layer vs. temperature calculated using formula (33) for the parameters presented in the text.

For the thermal generation of the defects (e.g., the laser-induced generation), the point-defect concentration in the stressed layer is represented as

$$N_{d0} = n_a \exp\left(-\frac{E_d - V_d\sigma_\parallel}{k_B T}\right), \tag{31}$$

where n_a is the atomic concentration in the crystal, E_d is the energy needed for the generation of a point defect, and V_d is the activation volume. Then, we find the maximum growth rate using expression (30)

$$\lambda_m = \frac{D_d}{l_\parallel^2}\left(\left(\frac{N_{eq}\nu\theta_d^2}{k_B T}\frac{\exp(V_d\sigma_\parallel/k_B T)}{\sigma_\parallel}\right)^{1/2} - 1\right)^2 \times \mathrm{sgn}\left(\left(\frac{N_{eq}\nu\theta_d^2}{k_B T}\frac{\exp(V_d\sigma_\parallel/k_B T)}{\sigma_\parallel}\right)^{1/2} - 1\right), \tag{32}$$

where $N_{eq} = n_a\exp(-E_d/k_B T)$ is the equilibrium concentration of the point defects in the absence of the stress. Using expression (32) and the condition $\lambda_m > 0$, we derive an equation for critical stress σ_c in the layer above which the DD instability is developed:

$$\frac{\exp(V_d\sigma_c/k_B T)}{\sigma_c} = (k_B T/N_{eq}\nu\theta_d^2).$$

An approximate solution to this equation can be written as

$$\sigma_c = \frac{E_d}{V_d} + \frac{k_B T}{V_d}\ln\frac{\sigma_c k_B T}{n_a\nu\theta_d^2} \approx \frac{E_d}{V_d}\left(1 - \frac{k_B T}{E_d}\left|\ln\frac{E_d k_B T}{V_d n_a\nu\theta_d^2}\right|\right). \tag{33}$$

For $n_a = 5\times10^{22}$ cm^{-3}, $E_d = 1.1$ eV, $V_d = 10^{-22}$ cm^{-3}, $T = 600$ K, and the above values of the remaining parameters, we obtain the estimate $\sigma_c = 6\times10^9$ erg cm^{-3}. Quantity σ_c almost linearly decreases with an increasing temperature (Fig. 5).

4. BIMODAL NANOPARTICLE SIZE DISTRIBUTION FUNCTION

In the case of the MBE, the strain extrema in the seed surface DD structure that results from the superposition of the DD gratings with different periods Λ serve as the nucleation centers. The subsequent growth of nucleuses in these centers leads to the formation of the nanodot ensemble.

By way of example, we consider the (100) surface that exhibits two selected mutually orthogonal directions along which the vectors of the DD gratings are oriented. The superposition of two DD gratings with wave vectors $\mathbf{q}_1$ and $\mathbf{q}_2$ such that $|\mathbf{q}_1| = |\mathbf{q}_2| \equiv q$ and $\mathbf{q}_1 \perp \mathbf{q}_2$ yields a 2D periodic square superlattice of the strain extrema (nucleation centers) with the period $\Lambda = 2\pi/q$. If the intermode interaction is neglected in the linear regime of the DD instability, the resulting DD structure consists of a superposition of square superlattices with the periods $\Lambda = 2\pi/q$ and the magnitudes of the wave vectors of these gratings are selected by the maxima of the DD instability growth rate. The superlattices are independent of each other in the linear approximation.

We assume that the nucleation and growth of the particles are faster than the development of the DD instability so that these processes are adiabatically adjusted to the latter. Then, we arrive at an exponential (with respect to time) growth of the Fourier amplitudes of the DD gratings at whose extrema (strain maxima or minima) the fast growth of nanoparticles takes place.

Similarly, upon the laser etching, an enhanced and rapid material removal occurs at the minima of the surface relief formed by the DD gratings with amplitudes that exponentially increase with time. This similarity makes it possible to propose a universal derivation of the size distribution functions of the nanoscale surface nonhomogeneities resulting from the MBE and the laser etching.

Each surface 2D DD grating with period Λ in the superposition is considered as a crystal (a periodic square superlattice) whose regular superlattice sites are occupied by the nanoparticle nucleuses (compare with atoms that occupy the regular lattice sites in a crystal). As in the crystalline lattice, the free energy of the superlattice is minimized when a fraction of regular sites in the superlattice are vacant. The surface concentration n_v (in cm^{-2}) of such vacancies in the square superlattice with period Λ is given by the thermodynamic formula by analogy with a crystal:

$$n_{SV}(\Lambda) = \Lambda^{-2}\exp(-E_1(\Lambda)/k_B T),$$

where $E_1(\Lambda)$ is the bond energy of one nucleus at the regular superlattice site (the energy needed for the for-

mation of a vacancy). Then, the size distribution function of the nanoparticles is given by

$$n_{\mathrm{dot}}(\Lambda) = \Lambda^{-2} - n_{\mathrm{SV}}(\Lambda) = \Lambda^{-2}[1 - \exp(-E_1(\Lambda)/k_{\mathrm{B}}T)]. \quad (34)$$

In the adiabatic approximation with respect to the bending coordinate, we express the bond energy $E_1(\Lambda)$ (potential-well depth) in terms of the squared modulus of the Fourier-amplitude of the growing DD grating with $q = 2\pi/\Lambda$ (i.e., in terms of the growth rate $\lambda_{\mathbf{q}} = \lambda(\Lambda)$). For this purpose, we use the following expression for the DD interaction energy stored in the bending-deformed surface layer with thickness h:

$$W = -\int_S d\mathbf{r}\int_0^h dz\theta_{\mathrm{d}} n_{\mathrm{d1}}(\mathbf{r}, z)\xi(\mathbf{r}, z),$$

where S is the surface area of the layer. The Fourier-series expansion of the variables yields

$$W = -S\int_0^h dz\sum_{\mathbf{q}}\theta_{\mathrm{d}} n_{\mathrm{d}q}(z)\xi_{-q}(z) \equiv \sum_{\mathbf{q}} W_q. \quad (35)$$

Then, the energy of one superlattice is written as

$$W_q = -S\int_0^h dz\theta_{\mathrm{d}} n_{\mathrm{d}}(q, z)\xi_{-q}(z) = -S\frac{4\nu\theta_{\mathrm{d}}^2}{h\rho_{\mathrm{f}}c^2}(1 + \nu l_0^2 q^2)\frac{1}{[q^2 + l_{\parallel}^{-2}]}|N_{\mathrm{d}}(q, t)|^2. \quad (36)$$

Dividing W_q by the number of the regular superlattice sites S/Λ^2, we obtain the energy of one site:

$$W_1 \equiv W_q\Lambda^2/S = -\Lambda^2\frac{4\nu\theta_{\mathrm{d}}^2}{h\rho_{\mathrm{f}}c^2}(1 + \nu l_0^2 q^2)\frac{1}{[q^2 + l_{\parallel}^{-2}]}|N_{\mathrm{d}}(q, t)|^2 \equiv -E_{SV}(q), \quad (37)$$

where $E_{\mathrm{SV}}(q)$ is the bond energy of a nucleus at a regular superlattice site in the superlattice with wave number q. Quantity $E_{\mathrm{SV}}(q)$ determines the energy of the defect formation: the absence of a nucleus (vacancy denoted with subscript SV) at a regular site in the superlattice with wave number q.

The (in cm^{-2}) quasi-equilibrium concentration of vacancies $n_{\mathrm{SV}}(q)$ in the surface superlattice q is given by

$$n_{\mathrm{SV}}(q) = \Lambda^{-2}\exp(-E_{\mathrm{SV}}(q)/k_{\mathrm{B}}T). \quad (38)$$

Then, the concentration of the nanodot nucleuses in the superlattice q is represented as

$$n_{\mathrm{dot}}(q) = \Lambda^{-2} - n_{\mathrm{SV}}(q) = \Lambda^{-2}[1 - \exp(-E_{\mathrm{SV}}(q)/k_{\mathrm{B}}T)]. \quad (39)$$

When the condition $E_{\mathrm{SV}}(q)/k_{\mathrm{B}}T < 1$ is satisfied, we employ expression (39) allowing for $\Lambda = 2\pi/q$ and formula (37) and obtain

$$n_{\mathrm{dot}}(q, t) = \frac{4\nu\theta_{\mathrm{d}}^2}{h\rho_{\mathrm{f}}c^2k_{\mathrm{B}}T}(1 + \nu l_0^2 q^2)\frac{1}{[q^2 + l_{\parallel}^{-2}]}|N_{\mathrm{d}}(q, t)|^2. \quad (40)$$

We put $t = t_0$ in relationship (40) and use $|N_{\mathrm{d}}(q, t_0)|^2 = |N_{\mathrm{d}}(q, 0)|^2\exp(2\lambda_q t_0)$, where t_0 is a characteristic time of the nucleation, which depends on the type of the nanostructuring process and will be defined below. Then, we obtain the following formula for the desired distribution:

$$n_{\mathrm{dot}}(q, t_0) \approx \frac{4\nu\theta_{\mathrm{d}}^2}{h\rho_{\mathrm{f}}c^2k_{\mathrm{B}}T}(1 + \nu l_0^2 q^2) \times \frac{1}{[q^2 + l_{\parallel}^{-2}]}|N_{\mathrm{d}}(q, 0)|^2\exp(2\lambda_q t_0). \quad (41)$$

5. COMPARISON WITH EXPERIMENTAL RESULTS

We compare the theoretical predictions and the experimental results for the case of the MBE of the Ge nanodots on Si. The Ge lattice constant is greater than the Si lattice constant, so that the Ge layer (with thickness h of several monolayers, see caption to Fig. 1) deposited on the Si surface is exposed to compressive stress [9] and, hence, cannot be directly involved in the DD instability. However, the stress of the same magnitude and opposite sign is exerted on the underlying Si layer. It is known that the tensile stress leads to an increase in the small (about 10^{-15} cm^2 s) Ge diffusion coefficient in Si [10]. It can be demonstrated that the tensile stress penetrates into Si at a depth that is on the order of the Ge layer thickness h, so that the Ge atoms diffuse to Si at the same depth h. Thus, the strain-enhanced diffusion of Ge to Si gives rise to a defect-enriched stressed layer with thickness h with the Ge atoms that penetrate from the upper layer and serve as the mobile defects. This defect-enriched layer with thickness h is subjected to tensile lateral stress $\sigma_{\parallel} > 0$ and, hence, can directly participate in the DD instability, which leads to the formation of the DD gratings at the Ge–Si interface. The superposition of the DD gratings gives rise to a strain field on the surface of the Ge layer that is spatially matched with the superpositional strain field of the interface. The extrema of this strain field serve as the nanoparticle nucleation centers.

At the stage of the particle nucleation at the extrema (maxima or minima) of the strain field that is spatially matched with the corresponding interface DD grating with period Λ, a monolayer nucleus with lateral size Λ is formed due to the arrival of atoms from the atomic beam.

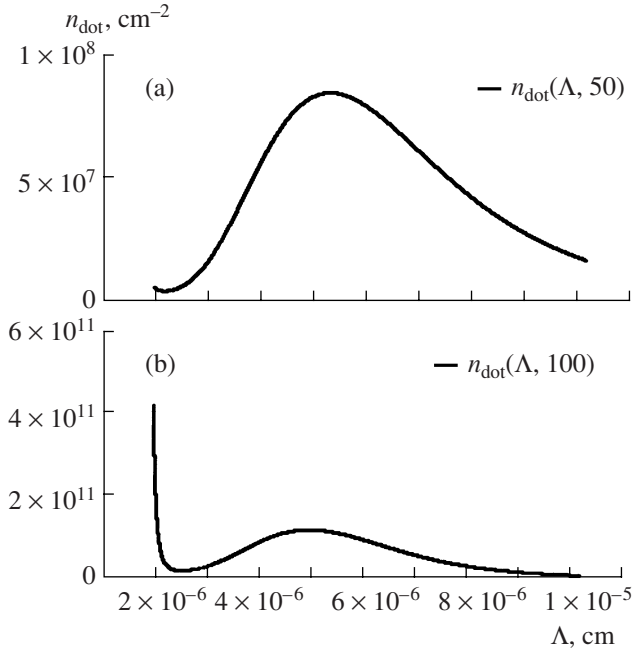

Fig. 6. Plot of the surface number density of nanoparticles n_{dot} vs. nanoparticle size Λ calculated using formula (43) and the parameters from the text for (a) $N_{d0}/N_c = 50$ and the curve of the growth rate versus Λ from Fig. 4a (t = 100 s) and (b) $N_{d0}/N_c = 100$ and the curve of the growth rate versus Λ from Fig. 4b (t = 100 s).

Characteristic time t_0, which enters expression (41), can be interpreted as the formation time of the monolayer:

$$t_0 = N_a/j_i, \tag{42}$$

where j_i (in atoms cm^{-2} s^{-1}) is the atomic flux density incident on the surface and N_a is the surface number density of atoms in the crystalline lattice ($N_a = (n_a)^{2/3}$). Then, using expressions (41) and (42), we obtain the final expression for the concentration of the nucleuses in the superlattice with wave vector q:

$$n_{dot}(q) = \frac{4\nu\theta_d^2}{h\rho_f c^2 k_B T}(1 + \nu l_0^2 q^2)\frac{1}{[q^2 + l_\parallel^{-2}]} \times \exp(2\lambda_q N_a/j_i)|N_d(q, 0)|^2, \tag{43}$$

where growth rate λ_q is given by formula (26). Substituting $q = 2\pi/\Lambda$ in expression (43), we obtain the size distribution function of the nucleuses: $n_{dot}(\Lambda) = (n_{dot}(q))_{q = 2\pi/\Lambda}$ (cm^{-2}).

Figure 6 demonstrates the dependences $n_{dot} = n_{dot}(\Lambda)$ for two values of the control parameter N_{d0}/N_c of the DD instability. The curves are plotted using expression (43) at $k_B T$ = 0.1 eV, $\theta_d = 10^2$ eV, $\rho_f c^2 = 7 \times 10^{11}$ erg cm^{-3}, ν = 1, $h = 10^{-6}$ cm, $l_d = 3 \times 10^{-7}$ cm, $\sigma_\parallel = 10^{10}$ erg cm^{-3}, and the uniform distribution of the initial (t = 0) fluctuations of the defect concentrations ($|N_d(q, 0)|^2$ = const and $N_d(q, 0) = 10^{16}$ cm^{-3}) with respect to q. The comparison of Figs. 1 and 2 with Fig. 6b shows that the shape of the calculated bimodal distribution function is similar to the shape of the experimental distribution function: a relatively broad quasi-symmetric maximum in the range of large nanoparticle sizes is supplemented by a narrower asymmetric maximum in the range of the small nanoparticle sizes. The asymmetry is due to the fact that the maximum corresponds to the limiting mode in the spectrum of bending modes and the dependence $n_{dot} = n_{dot}(\Lambda)$ rapidly reaches zero at $\Lambda < \Lambda_c = 2\pi/q_c = \pi/h$. Note that, at smaller ratios N_{d0}/N_c (closer to the threshold), the dependence of the growth rate on wave number q (i.e., on Λ) exhibits a single maximum (Fig. 4a). Correspondingly, the distribution function $n_{dot} = n_{dot}(\Lambda)$ also exhibits a single maximum at smaller ratios N_{d0}/N_c (Fig. 6a). Thus, the DD theory predicts a gradual transition from the unimodal nanoparticle size distribution to the bimodal distribution with an increase in N_{d0}/N_c. A transition from the unimodal nanoparticle size distribution to the bimodal distribution upon a variation in the control parameter of the process is typical of both the MBE and the nanostructuring induced by the laser radiation (Fig. 3).

Note the qualitative agreement of the above theoretical predictions regarding the positions of the two maxima for the distribution $n_{dot} = n_{dot}(\Lambda)$ as functions of thickness h of the surface layer and the experimental data from [5] (Fig. 1). It is seen that the long-wavelength maximum in the range of large sizes Λ is reached at Λ_{80} = 80 nm for $h = h_{12..5}$ = 12.5 ML (monolayers) and $h_{9.5}$ = 9.5 ML, whereas the maximum for an approximately twice thinner layer ($h_{6..5}$ = 6.5 ML and h = 5 ML) is reached at a twice smaller size Λ_{40} = 40 nm. It follows from expression (43) that the maxima of the $n_{dot} = n_{dot}(\Lambda)$ distribution almost coincide with the maxima of the growth-rate curve $\lambda_q = \lambda(\Lambda)$. The long-wavelength maximum of the growth rate is reached at $\Lambda = \Lambda_m = 2\pi/q_m \sim h$ (expression (29)). Thus, the DD theory predicts that the nanoparticle size at the distribution maximum in the range of large sizes is proportional to thickness h. This prediction is in agreement with the experimental data (Fig. 1). In accordance with the DD theory, the second (short-wavelength) maximum in the range of small sizes must be located at the particle size $\Lambda = 2h$. In the case under study 1 ML corresponds to 6.78×10^{14} atoms/cm^2 [5]. For the range 5.0 ML < h < 12.5 ML, the short-wavelength maxima must be located in the interval 4 < $2h$ < 10 nm. This is in agreement with the experimentally observed interval 5–14 nm (Fig. 1).

6. CONCLUSIONS

Thus, a new approach to the problem of the nanostructure self-organization on a solid surface is proposed. The approach is based on the concept of a

defect-induced instability involving the quasi-Lamb deformation waves that emerge in the near-surface layer (film) coupled with the quasi-Rayleigh deformation waves that emerge in the underlying elastic continuum (substrate). These interrelated surface static deformation waves are analogs of the classical acoustic surface waves (the Lamb wave that propagates in the plates and the Rayleigh wave that propagates along the surface of a semi-infinite medium). The generation and stationary maintenance of new-type coupled static deformation waves in the near-surface layer is due to the self-consistent distribution of defects resulting from the DD interaction via the defect deformation potential. The initial stage in the above scenario of the surface nanorelief self-organization involving the coupled static Lamb and Rayleigh waves is the formation of the stressed (stretched) surface nanolayer with thickness h that is enriched with mobile point defects. The same scenario that can be called a film on a substrate is also possible in the case of the self-organization of the surface relief microstructures. The extrema of the superpositional surface strain field induced by the continuum of the coupled Lamb–Rayleigh waves serve as the nanoparticle nucleation centers.

In this work, general expression (24) for the coefficient of the defect–bending coupling of the film is derived with regard to the reaction of the substrate (underlying elastic continuum), which leads to an increase in the effective bending rigidity of the film. It is demonstrated that the substrate reaction can be neglected at a relatively high lateral stress in the film. Thus, we prove the adequacy and indicate the applicability domain of the simplified model of the DD instability for a free film. This model was introduced in [11], where only the Lamb-wave instability was analyzed (see review [1] for the application of this model).

A distinctive feature of both film models is the fact that the lateral size of the nano- and microstructures is proportional to thickness h of the defect-enriched layer. The existence of such a universal linear dependence in the experimental results on the generation of the nano- and microstructures of the surface relief upon the laser and ion-beam irradiation of solid surfaces is demonstrated in [1]. Note that a similar linear dependence is observed in [6].

In [7, 12], we have recently studied an alternative scenario (with respect to the film model) of the formation of the surface relief nanostructures due to the self-organization of adatoms on a solid surface upon the interaction with the static Rayleigh wave. In this scenario, the lateral size of the surface relief nanostructures is proportional to the characteristic length of the deformation interaction of adatoms with each other. The length is represented in terms of the nonlocality parameter of the DD interaction l_d, which belongs to the nanometer range. It is demonstrated in [7] that two maxima emerge on the curve of the growth rate of the DD instability of the static Rayleigh wave versus the relief period when the normal and tangential surface forces that are exerted by the adatom system on the semi-infinite elastic continuum are simultaneously taken into account and the nonlocal character of the adatom–deformation interaction is accurately taken into account to the fourth-order terms in the expansion of the interaction integral.

In this work, we show that a similar (two-maximum) dependence of the growth rate on the relief period is observed for the DD instability of the coupled Lamb and Rayleigh waves. This makes it possible to propose a new interpretation of the two experimentally detected scales of modulation for the quasi-periodic surface relief that results from the laser and ion-beam irradiation of the semiconductor surfaces [1]. Recently, the existence of the second (micron) scale has been interpreted as a consequence of the DD instability of the second (thicker) defect-enriched layer that is formed owing to the defect diffusion from the thin near-surface layer to the bulk medium [1].

Note that, in this work, we develop a new approach to the calculation of the size distribution function for the nanoparticle ensemble that is formed due to the seed DD structure resulting from the surface DD instability. This unconventional approach involving the representation of the distribution function in terms of the DD instability growth rate is validated by the resulting scenario of a gradual transition from the unimodal nanoparticle size distribution to the bimodal distribution with an increase in the control parameter, which is in agreement with the experimental data (Fig. 3). The shapes of the resulting distributions and the maxima positions are also in agreement with the experimental results.

In this work, we do not consider the symmetry of the structures resulting from the development of the DD instability. In the case of an anisotropic surface (crystallographic anisotropy of elastic moduli, stress anisotropy, and diffusion anisotropy), the symmetry of the DD structure and the shape of the nucleation point correspond to the surface anisotropy [1, 7]. Therefore, a quasi-plane nucleus that emerges at the extremum of the seed DD structure on the (100) surface must be square shaped. On the other hand, a nanoparticle in the DD structure must have a circular base in the case of an isotropic surface [1, 7]. Assuming that the smaller the nanoparticle size, the stronger the crystal anisotropy effect on the nanoparticle shape, small nanoparticles in the short-wavelength (left-hand) maxima in Figs. 1 and 2 must be square-shaped, whereas large nanoparticles in the long-wavelength (right-hand) maxima can have circular bases. This conclusion corresponds to the experimental data in Fig. 2, where small particles (left-hand maximum) represent pyramids with square bases and large particles (right-hand maximum) represent hills with almost circular bases.

Thus, the DD scenario of the formation of a nanoparticle ensemble upon MBE is as follows. First, a

latent structure of the extrema of the long-range superpositional deformation field is generated at the surface owing to the DD instability and the excitation of the coupled static Lamb–Rayleigh waves. The atoms from the beam incident on the surface are deposited at a relatively high probability at the extrema of the surface deformation field and generate the nucleuses at the corresponding sites. In the case of the MBE, the distribution and shape of the nucleuses visualize the latent structure of the extrema in the superpositional strain field on the surface.

In the case of the multipulse laser etching, the material removal at the extrema of the DD field takes place at the maximum (or minimum) rate. The resulting distribution and the shape of hills and wells at the surface relief also visualizes the latent structure of the extrema in the superpositional DD field on the surface [1]. A universal mechanism of the formation of the surface DD field with a cellular structure via the development of the surface DD instability in various technological processes of the surface processing involving the generation of mobile point defects in a thin near-surface layer indicates the universal character of the DD mechanism for the nano- and microstructuring of solid surfaces.

Finally, note the drastic differences between the above DD mechanism for the instability of the stressed (stretched) surface layer involving the coupled Lamb–Rayleigh waves and the instability of the stressed (compressed) surface layer in accordance with the Asaro–Tiller–Grinfeld (ATG) effect [13, 14], which is normally used to interpret the threshold transition from a flat surface to a profiled surface of the layer deposited upon MBE [3]. In the ATG effect, the surface nanorelief results from the competition of the deformation energy and the surface energy of a solid in the presence of an external pressure. Defects do not play any role in the ATG effect. In the case of the ATG instability, the period of the surface relief modulation is given by [3]

$$\Lambda = \frac{1-\sigma_P}{2G(1+\sigma_P)^2}\frac{\pi\gamma}{\xi_0^2}, \quad (44)$$

where σ_P is the Poisson coefficient of the material, G is the shear modulus, γ is the surface-tension coefficient, and ξ_0 is the deformation related to the misfit stress between the growing layer and the substrate. The comparison of formulas (29a) and (44) shows that the main qualitative difference between the DD and ATG predictions lies in the absence of the proportionality of the relief modulation period to thickness h of the growing layer in the ATG interpretation. In contrast, the linear dependence of the relief modulation period on layer thickness h (the wavelength of the static Lamb wave) is a salient characteristic feature of the DD instability. Note also that the wavelength of the acoustic bending Lamb wave depends on the thickness of the propagation layer. Both dependences follow from the dependence of the bending rigidity of the layer on its thickness h (expression (9)).

REFERENCES

1. V. I. Emel'yanov, Laser Phys. **18**, 682 (2008).
2. V. Schukin and D. Bimberg, Rev. Mod. Phys. **71**, 1125 (1999).
3. J. Stangl, V. Holy, and G. Bauer, Rev. Mod. Phys. **76**, 725 (2004).
4. I. A. Viktorov, *Acoustic Surface Waves in Solids* (Nauka, Moscow, 1981) [in Russian].
5. S. A. Chaparro, J. Drucker, Y. Zhang, et al., Phys. Rev. Lett. **83**, 1199, 1999.
6. S. J. Henley, J. D. Carey, and S. R. P. Silva, Phys. Rev. B **72**, 195408 (2005).
7. V. I. Emel'yanov and A. I. Mikaberidze, Phys. Rev. B **72**, 235407 (2005).
8. L. D. Landau and E. M. Lifshitz, *Theory of Elasticity* (Nauka, Moscow, 1987; Pergamon, Oxford, 1986).
9. J. Walz, A. Greuer, G. Welder, et al., Appl. Phys. Lett. **73**, 2579, 1998.
10. Y. S. Lim, J. Y. Lee, H. S. Kim, and D. W. LeMoon, Appl. Phys. Lett. **80**, 2481 (2002).
11. V. I. Emel'yanov, in *Nonlinear Waves: Lectures at the Seventh All-Union School on Nonlinear Waves, Gorky, Russain, 1987* (Nauka, Moscow, 1989), p. 198.
12. V. I. Emel'yanov, Quantum Electron. **36**, 489 (2006).
13. R. J. Asaro and W. A. Tiller, Metall. Trans. **3**, 1789 (1972).
14. M. A. Grinfeld, Sov. Phys. Dokl. **31**, 831 (1986).